Band Structure Engineering of Interfacial Semiconductors Based on Atomically Thin Lead Iodide Crystals

Yan Sun, Zishu Zhou, Zhen Huang, Jiangbin Wu, Liujiang Zhou, Yang Cheng, Jinqiu Liu, Chao Zhu, Maotao Yu, Peng Yu, Wei Zhu, Yue Liu, Jian Zhou, Bowen Liu, Hongguang Xie, Yi Cao, Hai Li, Xinran Wang, Kaihui Liu, Xiaoyong Wang, Jianpu Wang, Lin Wang,* and Wei Huang*

To explore new constituents in two-dimensional (2D) materials and to combine their best in van der Waals heterostructures is in great demand as being a unique platform to discover new physical phenomena and to design novel functionalities in interface-based devices. Herein, PbI_2 crystals as thin as a few layers are synthesized, particularly through a facile low-temperature solution approach with crystals of large size, regular shape, different thicknesses, and high yields. As a prototypical demonstration of band engineering of PbI_2-based interfacial semiconductors, PbI_2 crystals are assembled with several transition metal dichalcogenide monolayers. The photoluminescence of MoS_2 is enhanced in MoS_2/PbI_2 stacks, while a dramatic photoluminescence quenching of WS_2 and WSe_2 is revealed in WS_2/PbI_2 and WSe_2/PbI_2 stacks. This is attributed to the effective heterojunction formation between PbI_2 and these monolayers; type I band alignment in MoS_2/PbI_2 stacks, where fast-transferred charge carriers accumulate in MoS_2 with high emission efficiency, results in photoluminescence enhancement, and type II in WS_2/PbI_2 and WSe_2/PbI_2 stacks, with separated electrons and holes suitable for light harvesting, results in photoluminescence quenching. The results demonstrate that MoS_2, WS_2, and WSe_2 monolayers with similar electronic structures show completely distinct light–matter interactions when interfacing with PbI_2, providing unprecedented capabilities to engineer the device performance of 2D heterostructures.

Heterostructure is a versatile platform to investigate physical phenomena and to build functional devices, owing to the rich physics occurring at the 2D interface between different materials. The emergence of 2D materials—with strong confinement in one dimension and full freedom in the other two dimensions—has created a truly 2D physics world that reveals many unusual properties and new phenomena. The growing amounts of 2D semiconductors, along with the alterable combination of them in van der Waals (vdWs) heterostructures by means of sophisticated assembly techniques, have offered great flexibility in their band engineering and broad application prospects in optoelectronic devices such as on-chip photodetectors, light emitting diodes, and single photon emitter.

As a widely studied group in 2D materials, transition metal dichalcogenides (TMDs), particularly in the form of monolayers (for instance MoS_2, WS_2, and WSe_2), possess many extraordinary

Y. Sun, Z. Zhou, Z. Huang, M. Yu, Y. Liu, B. Liu,
H. Xie, Y. Cao, Prof. H. Li, Prof. J. Wang, Prof. L. Wang,
Prof. W. Huang
Key Laboratory of Flexible Electronics (KLOFE) & Institute
of Advanced Materials (IAM)
Jiangsu National Synergetic Innovation Center
for Advanced Materials (SICAM)
Nanjing Tech University (NanjingTech)
30 South Puzhu Road, Nanjing 211816, China
E-mail: iamlwang@njtech.edu.cn; iamwhuang@nwpu.edu.cn

Dr. J. Wu
Ming Hsieh Department of Electrical Engineering
University of Southern California
Los Angeles, CA 90089, USA

Dr. L. Zhou, Dr. W. Zhu[+]
Center for Nonlinear Studies and Theoretical Division
Los Alamos National Laboratory
Los Alamos, NM 87545, USA

The ORCID identification number(s) for the author(s) of this article
can be found under https://doi.org/10.1002/adma.201806562.

[+]Present address: Westlake Institute of Advanced Study, Westlake
University, Hangzhou 310024, China

Y. Cheng, Prof. K. Liu
State Key Laboratory for Mesoscopic Physics
School of Physics Department
Peking University
Beijing 100871, China

J. Liu, Prof. X.-Y. Wang
National Laboratory of Solid State Microstructures
School of Physics
Nanjing University
Nanjing 210093, China

Dr. C. Zhu
Center for Programmable Materials
School of Materials Science and Engineering
Nanyang Technological University
Singapore 639798, Singapore

Dr. P. Yu
School of Materials Science and Engineering
Sun Yat-sen University
Guangzhou 510275, China

J. Zhou, Prof. X.-R. Wang
National Laboratory of Solid-State Microstructures
School of Electronic Science and Engineering Collaborative
Innovation Center of Advanced Microstructures
Nanjing University
Nanjing 210093, China

properties such as good photoluminescence (PL) performance and extremely large coulomb interactions.[1,2] More importantly, these physical properties can be easily tuned by band alignment, strain effect, doping level, and the surrounding environment, which provides extensive possibilities to implement heterostructure engineering based on TMD monolayers.[3–7] The strong p–d orbital hybridization in TMDs near the Fermi energy level affects the band alignment and charge transfer between interfaces; as a result, the PL behavior of TMDs can be tuned.[8–11] Meanwhile, most TMD/TMD heterostructures exhibit type II band alignment that is favorable to light harvesting,[12] as characterized by the observable interlayer excitons and PL quenching.[13–18] Even though both type I and type II band alignment could be formed by interfacing black phosphorus (BP) with TMDs, the PL of TMDs is also quenched because of the narrower bandgap of BP.[19] To date, the enhanced PL emission of TMDs could be achieved with combination of boron nitride (BN), perylene tetracarboxylic dianhydride, ZnO nanorods, and metal nanoparticles, as a result of the ultrasmooth and chemically inert surface of BN, energy transfer between the organic–inorganic interface, strain relaxation, and surface plasmon effect, respectively.[20–25] Therefore, it is challenging but desirable to have a general strategy—by means of interfacing one type of 2D semiconductor—to design distinct functionalities on similar types of TMDs via manipulating the charge transfer flow in their heterostructures.
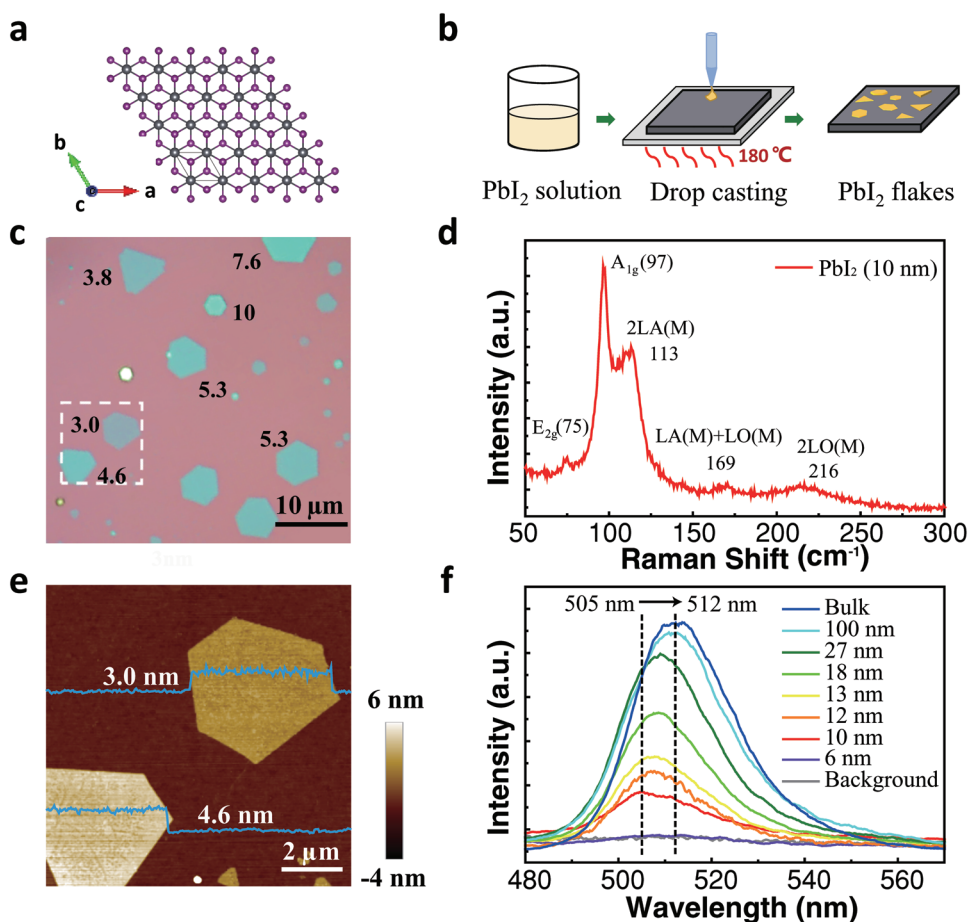
Also, there is always a strong demand for new types of 2D semiconductors that exhibit wide tunability and new optoelectronic properties. As a result, we turn our eyes to PbI_2, a layered semiconductor with a large bandgap around 2.5 eV in visible range.[26,27] PbI_2 bulk crystals have good applications in X-ray or γ-ray detection, as well as high-efficiency photodetectors and lasers at room temperature.[28–31] Moreover, PbI_2 is commonly used as a precursor of lead halide perovskite,[32] a "star" material for building high-performance photovoltaic devices and ligh-emitting diodes.[33–36] The realization of 2D PbI_2 would facilitate us to further design and grow a variety of 2D perovskites, which should show unprecedented potential in ultrathin optoelectronic devices of high compactness and high efficiency. Similar to TMDs, PbI_2 has hexagonal crystalline pattern with a lead atom layer sandwiched between two layers of iodide atoms, featured by strong covalent in-plane bonding and weak vdWs interactions between layers.[26,37,38] The hexagonal lattice structure of layered PbI_2 is depicted in **Figure 1**a. The lattice constants ($a = b = 4.559$ Å and $c = 6.990$ Å) are in good conformity with those of TMDs.[26] More importantly, PbI_2 manifests itself as a p-type semiconductor, while most TMDs like MoS_2 and WS_2 prefer to reveal n-type behavior.[39,40] Thus, the integration of PbI_2 with different TMDs can form a rich variety of p–n junctions as the basic building blocks of modern electronic devices. The congruence between PbI_2 and TMDs intrigues us to introduce PbI_2 into 2D system, and to fabricate TMD/PbI_2 heterostructures as a preliminary attempt of band structure engineering based on atomically thin PbI_2 crystals.

In this work, the synthesis and characterization of 2D PbI_2 and their interfacial interactions with several types of monolayer TMDs are under investigation. We have fabricated atomically thin PbI_2 flakes with large size, high crystallinity, and hexagonal/triangle shape via a facile solution processing method at atmosphere. As a good example of flexible interface engineering of 2D hybrid system based on PbI_2, we have transferred several TMD monolayers (taking MoS_2, WS_2, and WSe_2 for example) on top of PbI_2 flakes to assemble TMD/PbI_2 heterostructures, and then systematically investigated their optical properties tuned by different interlayer interactions. An enhanced PL emission of MoS_2 is observed in MoS_2/PbI_2 stacks, but conversely, a dramatic PL quenching of WS_2 and WSe_2 is revealed in WS_2/PbI_2 and WSe_2/PbI_2 stacks. As confirmed by first-principles calculations, we attribute these observations to type I band alignment in MoS_2/PbI_2 stacks, but type II in WS_2/PbI_2 and WSe_2/PbI_2 stacks, as corresponding to different charge carrier transfer processes in TMD/PbI_2 heterostructures. Our results provoke research effort in PbI_2 atomically thin crystals serving as a building block of vdWs heterostructures, which may further enlarge their applications in on-chip optoelectronic devices, such as single photon emitters, light-emitting diodes, and photodetectors.

In general, several kinds of methods have been applied to fabricate PbI_2 nanosheets, including mechanical exfoliation, physical vapor deposition (PVD), and solution process.[30,41,42] In contrast to exfoliation and PVD, solution method has the advantages of high productivity, simple operation and low manufacture cost, and the as-grown crystals are of good crystalline quality, regular shapes, and uniform surface.[34,42] But to date, it still remains a big challenge to synthesize atomically thin PbI_2 flakes via solution process. Herein, with the precise control of the concentration of PbI_2 precursor solution as well as crystalline nucleation rate, we have successfully obtained PbI_2 crystals down to atomic scale as thin as mono or few layers. Figure 1b briefly illustrates the preparation process: we first drop cast saturated PbI_2 aqueous solution onto a plasma-cleaned Si/SiO_2 substrate, and subsequently heat the substrate to 180 °C within 5 min to assist PbI_2 flakes with nucleation (see more details in the Experimental Section). The whole process is simple and quick, which avoids the rigorous conditions of high temperature and vacuum environment as required by PVD method, and the uncontrollability of the flake thickness, shape, and productivity in exfoliation process. The high yields and good morphology of our grown PbI_2 flakes can be revealed by characterizations of optical microscope and atomic force microscopy (AFM). From the optical image in Figure 1c, abundant PbI_2 flakes with different thickness are fully deposited on the substrate, exhibiting regular hexagonal or triangle shape with sharp edge. Figure 1e is an AFM scanning image of the selected region marked by white dashed lines in Figure 1c, suggesting the ultraflat and smooth surface of PbI_2 flakes. The height profile indicates that these two typical PbI_2 flakes are around 3.0 and 4.6 nm thick, respectively. Due to the absorbed water layer and other molecules on the substrates, there might be a small deviation between the real and the AFM-measured thickness of PbI_2 flakes, as also can be seen in other 2D materials.[43,44]

Optical measurements enable us to further check the physical properties of these as-grown PbI_2 flakes. Figure 1d shows the Raman spectra of a typical PbI_2 flake of 10 nm

Prof. W. Huang
Shaanxi Institute of Flexible Electronics (SIFE)
Northwestern Polytechnical University (NPU)
127 West Youyi Road, Xi'an 710072, Shaanxi, China

Figure 1. a) The hexagonal lattice of PbI_2 from top view. The dark gray balls represent lead (Pb) atoms and the purple balls represent iodine (I) atoms. b) Schematic illustration of synthesizing atomically thin PbI_2 flakes via solution method. PbI_2 aqueous solution was prepared and drop-cast onto Si/ SiO_2 substrate, followed by heating the substrate to 180 °C within 5 min to assist PbI_2 flakes to nucleate. c) The optical image of the as-grown PbI_2 flakes with regular hexagonal or triangle shape with sharp edge. The labeled numbers represent the thickness of the corresponding flakes. Scale bar: 10 µm. d) The Raman spectra of a typical 10 nm thick PbI_2 flake excited by 532 nm laser. e) Atomic force microscopy image of the selected region outlined by white dashed lines in (c) confirms the smooth and flat surface of PbI_2 flakes. The height profile of the two flakes indicates that their thickness is around 3.0 and 4.6 nm, respectively. Scale bar: 2 µm. f) The photoluminescence spectra of PbI_2 flakes with different thicknesses measured at room temperature. With decreasing the crystal thickness, the position of emission peak has a continuous blueshift and the intensity decreases correspondingly.

thick excited by 532 nm laser (around 2.33 eV). The characteristic peaks around 97 and 113 cm^{-1} can be determined as A_{1g} and 2LA(M) (overtone of the LA phonon at the M point of first Brillouin zone) vibration modes, respectively, and the LA(M) + LO(M) (169 cm^{-1}) and 2LO(M) (216 cm^{-1}) Raman peaks are also visible, in line with the previous reports of PbI_2.[41,45] Furthermore, we could distinguish the subtle split of E_{2g} (75 cm^{-1}) vibration peak as an indication of the 4H phase of our PbI_2 flakes.[37] Thickness-dependent PL of PbI_2 flakes was carried out under 290 and 4 K, and the results are shown in Figure 1f and Figure S1 (Supporting Information), respectively. For PbI_2 bulk crystals, a strong emission peak around 512 nm is observed. Owing to quantum confinement, the position of PL emission peak shows a continuous blueshift as the thickness decreases, accompanied with the gradually dropped intensity. When it comes to few layers, the PL signal becomes too weak to recognize at room temperature, because of the direct–indirect semiconductor transition occurred around three layers.[45,46] However, the PL emission of PbI_2 as thin as few layers at cryogenic temperatures is still very remarkable with three distinct peaks, as corresponding to excitonic emission, traps states in bulk, and traps related to surface quality.[47]

On the basis of atomically thin PbI_2 crystals with high yields and good quality, we further interface MoS_2 monolayers with these PbI_2 flakes. The thickness of the chosen PbI_2 flakes for MoS_2/PbI_2 stacks is within the range of around 3–9 nm (although we could synthesize even thinner flakes), which are more than four layers and less than 12 layers, as they can keep 2D features and possess a direct bandgap simultaneously.[45,46] For the same reason, MoS_2 monolayers are selected instead of thicker ones.[1] The exfoliated MoS_2 monolayers are used to cap the as-grown PbI_2 flakes by dry transfer method to construct vdWs heterostructures, as schematically shown in **Figure 2**a (see the Experimental Section). The side view of MoS_2/PbI_2 stacks is depicted by a cartoon image in Figure 2b. Figure 2d presents an optical microscope image of one heterostructure sample, in which a large continuous MoS_2 piece covers several PbI_2 flakes. The contours of the PbI_2 flakes are outlined by black dashed lines, and two of them
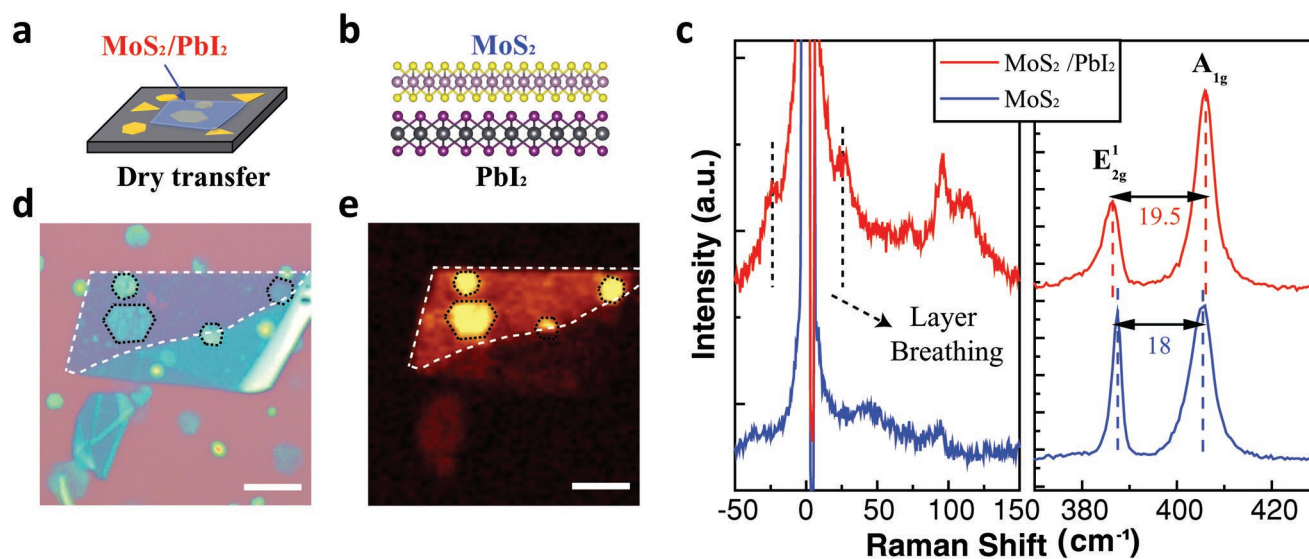
Figure 2. a) Schematic image of MoS_2/PbI_2 stacks. The exfoliated MoS_2 monolayer is used to cap the as-grown PbI_2 flakes by dry transfer method. b) The lattice structure of MoS_2/PbI_2 stacks from side view. The lilac balls represent molybdenum (Mo) atoms and the yellow balls represent sulfur (S) atoms. c) The Raman spectra of pristine MoS_2 monolayer and MoS_2/PbI_2 stacks. d) Optical image of MoS_2/PbI_2 stacks with a large monolayer MoS_2 piece capping several PbI_2 flakes. The hexagonal PbI_2 flakes are marked by black dashed lines, and two of them are completely encapsulated by the monolayer MoS_2 whose outlines are denoted by white dashed lines. Scale bar: 5 μm. e) The photoluminescence mapping image of the same heterostructure shown in (d), spectrally integrated from 1.79 to 1.88 eV, in which the brilliant yellow denotes the high photoluminescence emission intensity. Scale bar: 5 μm.

are completely encapsulated by the monolayer MoS_2. The thickness of the larger one (about 8 μm²) is around 3.0 nm, and the other (about 3 μm²) is around 12.4 nm. Raman spectroscopy has been extensively used to study the effects of doping, strain, and interlayer interactions in TMDs.[3,4,48,49] As for the Raman spectrum of MoS_2/PbI_2 stacks shown in Figure 2c, the Raman peaks around 96 and 113 cm⁻¹ assigned to PbI_2 are still observable. When comparing with the Raman spectrum of the monolayer MoS_2 alone, in the MoS_2/PbI_2 stacks the A_{1g} peak has a blueshift ≈0.5 cm⁻¹ and the E^1_{2g} peak has a redshift ≈1 cm⁻¹. It may have many origins such as vdWs interactions, strain, doping, and laser-induced thermal effect.[23,49–53] A very possible scenario for the change of the Raman peak positions is the strong interlayer interaction between MoS_2 and PbI_2, as evidenced by the appearance of layer breathing mode in the ultralow frequency Raman spectra (denoted in Figure 2c). It is known that the layer breathing mode could only be seen in 2D heterostructures with good quality interface.[54] Figure 2e illustrates the PL emission mapping under 488 nm laser excitation with integration from 1.79 to 1.88 eV of the entire heterostructure. Strong PL signals are detected in the monolayer MoS_2 region, but even more enhanced PL emission in the regions of MoS_2/PbI_2 stacks, as can be seen from that the brilliant yellow profile of PbI_2 flakes under MoS_2 is quite clear.

Figure 3a carefully compares the PL spectra of the sample shown in Figure 2, with the signal taken from the MoS_2 alone and MoS_2/PbI_2 region, respectively. When forming MoS_2/PbI_2 stacks, the PL signal assigned to monolayer MoS_2 shifts to a high energy position, and the intensity increases by several folds. We have fabricated more than ten samples, all of which show similar optical behavior with the increasing amplitude in the range of 160%–600% if calculated by $\frac{PL(TMD/PbI_2)}{PL(TMD)}$.

Furthermore, similar PL behavior is also observed in PbI_2/MoS_2 stacks in which PbI_2 is on top of MoS_2 (see Figure S3, Supporting Information). To better understand the origin of these changes, we fit the PL spectra with three Lorentzian peaks, as corresponding to negative trion (X⁻) at ≈1.82 eV, neutral exciton (X) at ≈1.86 eV, and B exciton at ≈1.98 eV.[4,5] From the analysis, the proportion of the trion (X⁻) is greater than that of the neutral exciton (X) in monolayer MoS_2 alone, because of the n-type trait of MoS_2.[40] With the addition of PbI_2, the PL enhancement and blueshift of MoS_2 emission peak is because the neutral exciton (X) emission significantly increases, while the trion (X⁻) emission keeps almost unchanged. This clearly reveals that the doping effect is not the main origin of the PL enhancement of MoS_2 in MoS_2/PbI_2 heterostructures, very differently from other 2D systems with high emission of MoS_2. For instance, in MoS_2/BN heterostructures, the underlying BN flakes prevent the n-type doping effect of MoS_2 from SiO_2 substrates effectively—which causes the reduction of trion emission (X⁻) and then relative enhancement of neutral exciton emission (X)—leading to the stronger PL signal of MoS_2 (the detailed comparison can be seen in Figure S4, Supporting Information).[54,55] In MoS_2/PbI_2 heterostructures the inrush of external electrons and holes rather than doping itself accounts for the enhanced emission of the neutral exciton (X). In order to figure out the origin of these charge carries, we have carried out density functional theory (DFT) calculations on the constructed heterostructures (see more details in the Experimental Section and Figure S5, Supporting Information). As shown in Figure 3b, MoS_2/PbI_2 heterostructures show type I band alignment owing to the large bandgap of PbI_2 and strong built-in potentials. The excitons originating from the absorption of photons in PbI_2 partly separate under the effect of built-in potentials, and quickly accumulate in MoS_2 by charge transfer process. These exotic

**ADVANCED
SCIENCE NEWS**

www.advancedsciencenews.com

**ADVANCED
MATERIALS**

www.advmat.de
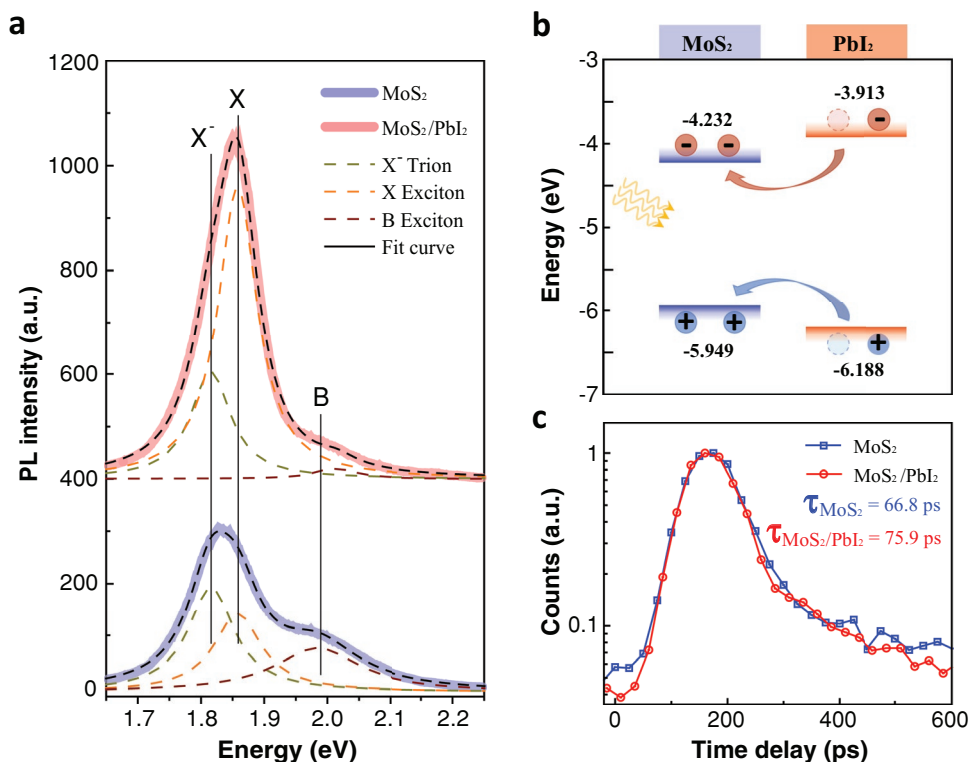
Figure 3. a) The photoluminescence spectra of pristine MoS_2 monolayer and MoS_2/PbI_2 stacks with 488 nm excitation, in the analysis of three Lorentzian peaks corresponding to negative trion (X^-) at $\approx$1.82 eV, neutral exciton (X) at $\approx$1.86 eV, and B exciton at $\approx$1.98 eV. In MoS_2/PbI_2 stacks, the position assigned to MoS_2 shifts to high energy, and the total intensity increases by several folds with the X^- emission unchanged. b) Type I band alignment for MoS_2/PbI_2 stacks with illustratively showing the transfer of photoexcited carriers within the heterostructure, as calculated by density functional theory. The inrush of electrons and holes from PbI_2 to MoS_2 makes the contribution from neutral exciton emission (X) increase. c) The time-resolved photoluminescence spectra of pristine MoS_2 monolayer and MoS_2/PbI_2 stacks, showing that the photoluminescence lifetime of MoS_2 in MoS_2/PbI_2 stacks ($\approx$75.9 ps) is almost the same with that of pristine MoS_2 ($\approx$66.8 ps).

carries occupy the neutral exciton (X) energy level of MoS_2 and release energy by radiative recombination ultimately, leading to the improvement and blueshift of PL emission of MoS_2. It is also noted that in MoS_2/PbI_2 stacks, the B exciton emission peak drops and moves to a higher energy level. Take the existence of heavy Pb atoms in PbI_2 and the interlayer coupling between MoS_2 and PbI_2 into consideration, the change of B exciton emission might be caused by strong spin–orbital coupling. Furthermore, we find that the PL behavior of MoS_2 on top of two PbI_2 flakes with different thicknesses is almost the same (see Figure S7, Supporting Information), and thus we think that the optical interference effect of PbI_2 with different thicknesses is subtle. Time-resolved photoluminescence (TRPL) is highly suitable to analyze and determine the fast charge carrier dynamics in semiconductors. In Figure 3c of TRPL spectra, the PL lifetime of MoS_2 in MoS_2/PbI_2 stacks ($\approx$75.9 ps) has little change compared with that of MoS_2 alone ($\approx$66.8 ps), as MoS_2 plays an acceptor role in the heterostructure. The almost coincident rising edge indicates that the charge transfer process between PbI_2 and MoS_2 is too fast (less than 25 ps) to distinguish in our experimental setup. Unfortunately, we are unable to obtain any information about the PL lifetime of PbI_2 flakes, as the signal is too weak to detect.

As being typical members of TMDs, WS_2 and WSe_2 exhibit many similar behaviors to MoS_2. Following this rationale, we

further use monolayer WS_2 and WSe_2 instead of MoS_2 to build WS_2/PbI_2 and WSe_2/PbI_2 stacks. The Raman spectra of these stacks excited by 488 nm laser are shown in **Figure 4**a. The emergence of the Raman peaks characteristic of WS_2 and WSe_2 also occurs in heterostructures, indicating the high quality of the prepared stacks. Because of the interfacial interaction and the additional absorption by the PbI_2, the peak position of A_{1g} mode exhibits a redshift of $\approx$1.4 cm^{-1}, and the increasing resonant peak of 2LA(M) mode surpasses the one of E^1_{2g} mode in the Raman spectra of WS_2/PbI_2 stacks. In the Raman spectra of WSe_2/PbI_2 stacks, the peak positions of E^1_{2g} and A_{1g} modes keep the same with the case of isolated WSe_2, and the emergence of a new resonant Raman peak (LA(M) + ZA(M)) verifies the strong interaction between WSe_2 and PbI_2. In contrast to the PL enhancement in MoS_2/PbI_2 stacks, the PL emission of WS(Se)$_2$ in WS(Se)$_2$/PbI_2 stacks decreases (WS_2, 5%–40%; WSe_2, 4%–30% in all the samples we measured) with a redshift by about 10 meV (see Figure 4b,c). The optical image and PL mapping in Figure 4d,e intuitively show this PL quenching effect, where the WSe_2/PbI_2 region is dramatically dark compared to the bright zone of monolayer WSe_2 alone. Our DFT calculations (see Figure 4f) reveal that both WS_2/PbI_2 and WSe_2/PbI_2 heterostructures exhibit type II band alignment, so that the conduction band of the interface is originated from PbI_2 side and the valence band from WS_2 or WSe_2 side. The
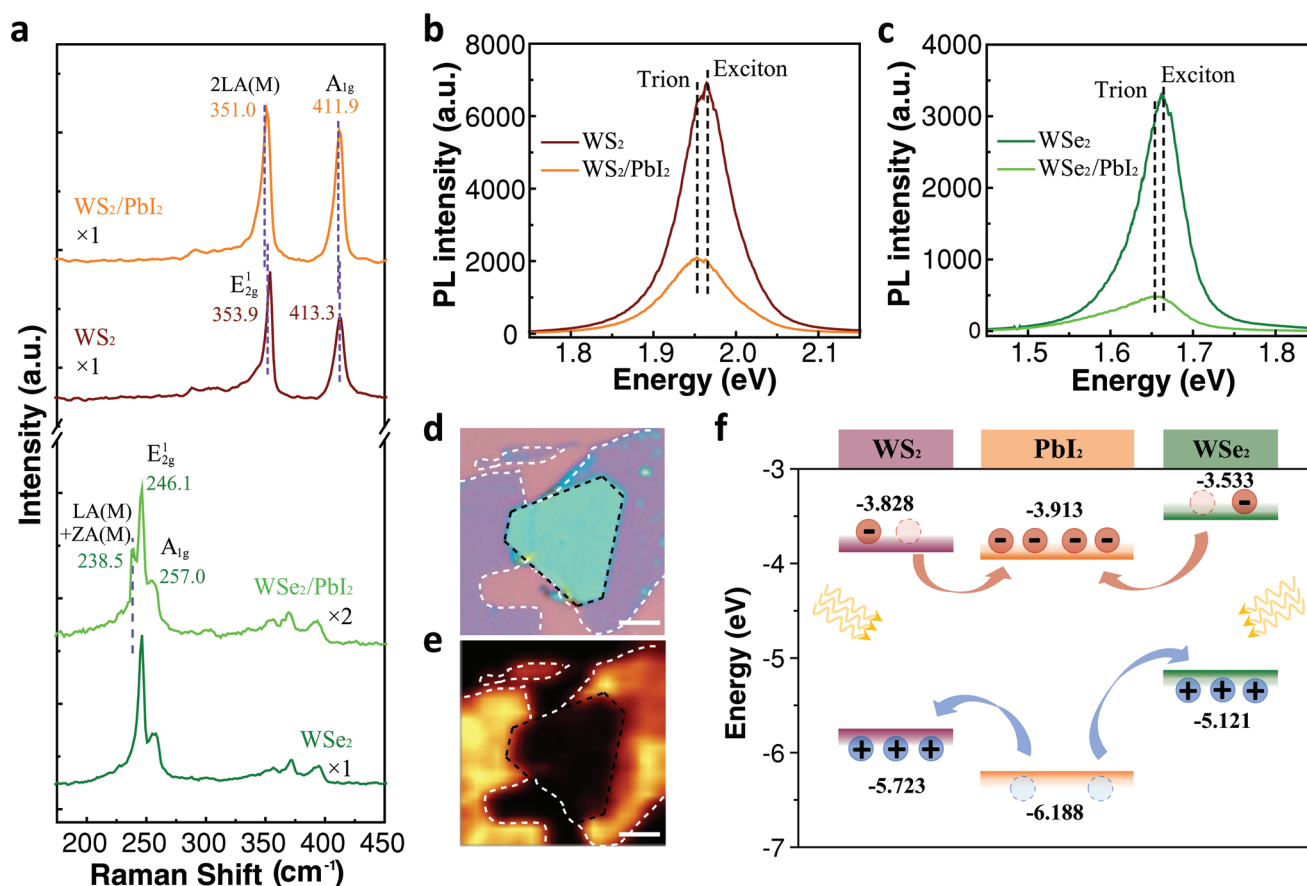
Figure 4. a) The Raman spectra of pristine WS(Se)$_2$ monolayer and WS(Se)$_2$/PbI$_2$ stacks. The redshift of A$_{1g}$ mode and the increasing resonant peak of 2LA(M) mode indicate the strong interaction between WS$_2$ and PbI$_2$ layers. The emergence of a new resonant Raman peak (LA(M) + ZA(M)) also verifies the strong interaction between WSe$_2$ and PbI$_2$ layers. b,c) The photoluminescence spectra of pristine WS$_2$ monolayer and WS$_2$/PbI$_2$ stacks (b), and pristine WSe$_2$ monolayer and WSe$_2$/PbI$_2$ stacks (c). In WS(Se)$_2$/PbI$_2$ stacks, the photoluminescence of WS(Se)$_2$ shows a significant quenching, as well as a redshift in peak position. d) Optical image of WSe$_2$/PbI$_2$ stacks with monolayer WSe$_2$ capping a big PbI$_2$ flake. The contour of the hexagonal PbI$_2$ flake is marked by black dashed lines, and the monolayer MoS$_2$ by white dashed lines. Scale bar: 3 µm. e) The photoluminescence mapping image of the same heterostructure shown in (d), spectrally integrated from 1.77 to 1.94 eV, in which the photoluminescence of WSe$_2$ is quenched on location of PbI$_2$. Scale bar: 3 µm. f) Type II band alignment for WS$_2$/PbI$_2$ and WSe$_2$/PbI$_2$ stacks, with the illustrative transfer of photoexcited carriers within the heterostructures as calculated by density functional theory. The conduction band minimum of the interface is originated from PbI$_2$ and the valence band maximum from WS(Se)$_2$. The separation of excitons leads to the photoluminescence quenching of WS(Se)$_2$ in WS(Se)$_2$/PbI$_2$ stacks.

different flow directions of electrons and holes lead to the loss of neutral excitons; as a result, the emission of trions with low-energy position becomes dominant. Therefore, the total decrease and redshift of WS(Se)$_2$ emission peak in WS(Se)$_2$/PbI$_2$ stacks are observed. The opposite effect of PbI$_2$ on MoS$_2$ and WS(Se)$_2$ also implies that the different types of band alignment (instead of doping effect) are the dominant factor of determining and manipulating the optical properties of TMD/PbI$_2$ interfacial semiconductors. Therefore, PbI$_2$ atomically thin crystals show great potential in the band structure engineering as a new building block of 2D heterostructures.

In summary, atomically thin PbI$_2$ flakes of high quality have been successfully synthesized for the first time. A series of atomic-scale heterostructures constructed by PbI$_2$ and TMD monolayers—namely MoS$_2$, WS$_2$, and WSe$_2$/PbI$_2$—are under investigation to illustrate the unprecedented possibilities and capabilities of 2D PbI$_2$ in the band structure engineering. The optical measurement results show that the addition of

PbI$_2$ brings distinctive impacts on different TMDs of similar electronic structure, originating from different types of band alignment. Concretely speaking, an enhanced PL of MoS$_2$ results from the high emission efficiency of accumulated charges in the form of type I band alignment in MoS$_2$/PbI$_2$ stacks, but the separated electron–hole pairs lead to the dramatically quenched PL effect of WS$_2$ or WSe$_2$ in type II WS$_2$/PbI$_2$ and WSe$_2$/PbI$_2$ stacks. Atomic-level PbI$_2$-based heterostructures provide us with more freedom to deterministically manipulate the semiconducting interface properties such as the exciton behavior and surface energy transfer process, by selecting the appropriate constituents in the vast family of 2D materials.

Experimental Section

Fabrication: PbI$_2$ precursor solution was prepared by dissolving PbI$_2$ powder (Sigma-Aldrich) in deionized water (1 mg mL^{-1}) and heated with stirring at 90 °C until PbI$_2$ powder was dissolved completely. Then the

solution was drop-cast on an oxygen-plasma-cleaned SiO_2/Si substrate at room temperature, followed by heating the substrate to 180 °C within 5 min to help PbI_2 nanosheets nucleate. The monolayer TMDs were obtained by mechanical exfoliation method and then transferred onto the pregrown PbI_2 flakes by polypropylene carbonate (PPC)-assisted dry transfer technique.

Characterization: The topography and height profile were measured by AFM (Park XE7) in noncontact mode. Micro-PL spectra of PbI_2 flakes were measured by 410 nm solid-state laser excitation source with the laser beam being focused to a spot size of ≈2 μm, and PL spectra of pristine TMDs and TMDs/PbI_2 stacks were excited by 488 nm continuous wave laser with the laser beam being focused to a spot size of ≈500 nm. The PL signals were recorded with a monochromator and a liquid-nitrogen-cooled charge-coupled device (CCD). The Raman spectra were acquired using a micro-Raman system (WITec alpha 300R) equipped with 1800 grooves per millimeter gratings and a liquid-nitrogen-cooled CCD detector. For TRPL measurements, the excitation pulse laser (410 nm beam, 100 fs, 80 MHz) was focused by a microscopic objective (100×; NA = 0.95) onto the sample at normal incidence. The backscattered signal filtered by a proper long pass was collected using time-correlated single-photon counting, which has a resolution of ≈25 ps. All the measurements were conducted under room temperature, unless stated otherwise.

Computational Details: The DFT calculations were carried out by using the Vienna ab initio Simulation Package (VASP).[56] The exchange correlation interaction was treated within the generalized gradient approximation parameterized by the Perdew, Burke, and Ernzerhof.[57] Electronic wave functions were built in the plane wave basis sets with a kinetic energy cutoff of 400 eV. All the atoms in models were fully optimized using the optimized Becke88 van der Waals functional until the force on each atom was less than 0.01 eV $Å^{-1}$.[58] The reciprocal space was sampled with a k-grid density of 0.02 × $2\pi Å^{-1}$ for the structure optimization and 0.01 × $2\pi Å^{-1}$ for the calculations of electronic structures. In our models, a vacuum layer of 20 Å was used to isolate neighboring periodic images in all systems. Four-layer PbI_2 was utilized to mimic the experimental PbI_2 flake. The thicker PbI_2 flake was not considered here since our test indicates that it has little effect on the band alignments of heterojunctions. It is important to mention that although DFT underestimates the electronic bandgap, it provides good agreement with the optical bandgaps in these low-dimensional systems.[59]

Supporting Information

Supporting Information is available from the Wiley Online Library or from the author.

Acknowledgements

Conflict of Interest

The authors declare no conflict of interest.

[1] A. Splendiani, L. Sun, Y. Zhang, T. Li, J. Kim, C. Y. Chim, G. Galli, F. Wang, *Nano Lett.* **2010**, *10*, 1271.

[2] K. F. Mak, C. Lee, J. Hone, J. Shan, T. F. Heinz, *Phys. Rev. Lett.* **2010**, *105*, 136805.

[3] H. J. Conley, B. Wang, J. I. Ziegler, R. F. Haglund Jr., S. T. Pantelides, K. I. Bolotin, *Nano Lett.* **2013**, *13*, 3626.

[4] S. Mouri, Y. Miyauchi, K. Matsuda, *Nano Lett.* **2013**, *13*, 5944.

[5] M. S. Kim, C. Seo, H. Kim, J. Lee, D. H. Luong, J. H. Park, G. H. Han, J. Kim, *ACS Nano* **2016**, *10*, 6211.

[6] J. S. Ross, S. Wu, H. Yu, N. J. Ghimire, A. M. Jones, G. Aivazian, J. Yan, D. G. Mandrus, D. Xiao, W. Yao, X. Xu, *Nat. Commun.* **2013**, *4*, 1474.

[7] K. F. Mak, K. He, C. Lee, G. H. Lee, J. Hone, T. F. Heinz, J. Shan, *Nat. Mater.* **2013**, *12*, 207.

[8] K. Zhao, Z. Deng, X. C. Wang, W. Han, J. L. Zhu, X. Li, Q. Q. Liu, R. C. Yu, T. Goko, B. Frandsen, L. Liu, F. Ning, Y. J. Uemura, H. Dabkowska, G. M. Luke, H. Luetkens, E. Morenzoni, S. R. Dunsiger, A. Senyshyn, P. Boni, C. Q. Jin, *Nat. Commun.* **2013**, *4*, 1442.

[9] G. Zhao, C. Lin, Z. Deng, G. Gu, S. Yu, X. Wang, Z. Gong, Y. J. Uemera, Y. Li, C. Jin, *Sci. Rep.* **2017**, *7*, 14473.

[10] N. R. Wilson, P. V. Nguyen, K. Seyler, P. Rivera, A. J. Marsden, Z. P. Laker, G. C. Constantinescu, V. Kandyba, A. Barinov, N. D. Hine, *Sci. Adv.* **2017**, *3*, e1601832.

[11] G.-B. Liu, W.-Y. Shan, Y. Yao, W. Yao, D. Xiao, *Phys. Rev. B* **2013**, *88*, 085433.

[12] B. Zheng, C. Ma, D. Li, J. Lan, Z. Zhang, X. Sun, W. Zheng, T. Yang, C. Zhu, G. Ouyang, G. Xu, X. Zhu, X. Wang, A. Pan, *J. Am. Chem. Soc.* **2018**, *140*, 11193.

[13] X. Hong, J. Kim, S. F. Shi, Y. Zhang, C. Jin, Y. Sun, S. Tongay, J. Wu, Y. Zhang, F. Wang, *Nat. Nanotechnol.* **2014**, *9*, 682.

[14] S. Tongay, W. Fan, J. Kang, J. Park, U. Koldemir, J. Suh, D. S. Narang, K. Liu, J. Ji, J. Li, *Nano Lett.* **2014**, *14*, 3185.

[15] M. H. Chiu, C. Zhang, H. W. Shiu, C. P. Chuu, C. H. Chen, C. Y. Chang, C. H. Chen, M. Y. Chou, C. K. Shih, L. J. Li, *Nat. Commun.* **2015**, *6*, 7666.

[16] P. Rivera, J. R. Schaibley, A. M. Jones, J. S. Ross, S. Wu, G. Aivazian, P. Klement, K. Seyler, G. Clark, N. J. Ghimire, J. Yan, D. G. Mandrus, W. Yao, X. Xu, *Nat. Commun.* **2015**, *6*, 6242.

[17] J. Zhang, J. Wang, P. Chen, Y. Sun, S. Wu, Z. Jia, X. Lu, H. Yu, W. Chen, J. Zhu, G. Xie, R. Yang, D. Shi, X. Xu, J. Xiang, K. Liu, G. Zhang, *Adv. Mater.* **2016**, *28*, 1950.

[18] M. Baranowski, A. Surrente, L. Klopotowski, J. M. Urban, N. Zhang, D. K. Maude, K. Wiwatowski, S. Mackowski, Y. C. Kung, D. Dumcenco, A. Kis, P. Plochocka, *Nano Lett.* **2017**, *17*, 6360.

[19] J. Yuan, S. Najmaei, Z. Zhang, J. Zhang, S. Lei, P. M. Ajayan, B. I. Yakobson, J. Lou, *ACS Nano* **2015**, *9*, 555.

[20] A. Boulesbaa, V. E. Babicheva, K. Wang, I. I. Kravchenko, M.-W. Lin, M. Mahjouri-Samani, C. B. Jacobs, A. A. Puretzky, K. Xiao, I. Ivanov, C. M. Rouleau, D. B. Geohegan, *ACS Photonics* **2016**, *3*, 2389.

[21] Y. Li, J. D. Cain, E. D. Hanson, A. A. Murthy, S. Hao, F. Shi, Q. Li, C. Wolverton, X. Chen, V. P. Dravid, *Nano Lett.* **2016**, *16*, 7696.

[22] M. R. Habib, H. Li, Y. Kong, T. Liang, S. M. Obaidulla, S. Xie, S. Wang, X. Ma, H. Su, M. Xu, *Nanoscale* **2018**, *10*, 16107.

**ADVANCED
SCIENCE NEWS**

www.advancedsciencenews.com

**ADVANCED
MATERIALS**

www.advmat.de

[23] S. Wang, X. Wang, J. H. Warner, *ACS Nano* **2015**, *9*, 5246.

[24] H. Jeong, H. M. Oh, A. Gokarna, H. Kim, S. J. Yun, G. H. Han, M. S. Jeong, Y. H. Lee, G. Lerondel, *Adv. Mater.* **2017**, *29*, 1700308.

[25] Z. Q. Wu, J. L. Yang, N. K. Manjunath, Y. J. Zhang, S. R. Feng, Y. H. Lu, J. H. Wu, W. W. Zhao, C. Y. Qiu, J. F. Li, S. S. Lin, *Adv. Mater.* **2018**, *30*, 1706527.

[26] I. C. Schlüter, M. Schlüter, *Phys. Rev. B* **1974**, *9*, 1652.

[27] A. S. Toulouse, B. P. Isaacoff, G. Shi, M. Matuchová, E. Kioupakis, R. Merlin, *Phys. Rev. B* **2015**, *91*, 165308.

[28] R. Street, S. Ready, K. Van Schuylenbergh, J. Ho, J. Boyce, P. Nylen, K. Shah, L. Melekhov, H. Hermon, *J. Appl. Phys.* **2002**, *91*, 3345.

[29] X. Liu, S. T. Ha, Q. Zhang, M. de la Mata, C. Magen, J. Arbiol, T. C. Sum, Q. Xiong, *ACS Nano* **2015**, *9*, 687.

[30] M. Zhong, L. Huang, H.-X. Deng, X. Wang, B. Li, Z. Wei, J. Li, *J. Mater. Chem. C* **2016**, *4*, 6492.

[31] J. Zhang, T. Song, Z. Zhang, K. Ding, F. Huang, B. Sun, *J. Mater. Chem.* **2015**, *3*, 4402.

[32] S. Chen, G. Shi, *Adv. Mater.* **2017**, *29*, 1605448.

[33] N. Wang, L. Cheng, R. Ge, S. Zhang, Y. Miao, W. Zou, C. Yi, Y. Sun, Y. Cao, R. Yang, Y. Wei, Q. Guo, Y. Ke, M. Yu, Y. Jin, Y. Liu, Q. Ding, D. Di, L. Yang, G. Xing, H. Tian, C. Jin, F. Gao, R. H. Friend, J. Wang, W. Huang, *Nat. Photonics* **2016**, *10*, 699.

[34] J. Liu, Y. Xue, Z. Wang, Z. Q. Xu, C. Zheng, B. Weber, J. Song, Y. Wang, Y. Lu, Y. Zhang, Q. Bao, *ACS Nano* **2016**, *10*, 3536.

[35] L. Niu, X. Liu, C. Cong, C. Wu, D. Wu, T. R. Chang, H. Wang, Q. Zeng, J. Zhou, X. Wang, W. Fu, P. Yu, Q. Fu, S. Najmaei, Z. Zhang, B. I. Yakobson, B. K. Tay, W. Zhou, H. T. Jeng, H. Lin, T. C. Sum, C. Jin, H. He, T. Yu, Z. Liu, *Adv. Mater.* **2015**, *27*, 7800.

[36] Y. Cao, N. Wang, H. Tian, J. Guo, Y. Wei, H. Chen, Y. Miao, W. Zou, K. Pan, Y. He, H. Cao, Y. Ke, M. Xu, Y. Wang, M. Yang, K. Du, Z. Fu, D. Kong, D. Dai, Y. Jin, G. Li, H. Li, Q. Peng, J. Wang, W. Huang, *Nature* **2018**, *562*, 249.

[37] R. Zallen, M. L. Slade, *Solid State Commun.* **1975**, *17*, 1561.

[38] M. Ando, M. Yazaki, I. Katayama, H. Ichida, S. Wakaiki, Y. Kanematsu, J. Takeda, *Phys. Rev. B* **2012**, *86*, 155206.

[39] R. Street, S. Ready, F. Lemmi, K. Shah, P. Bennett, Y. Dmitriyev, *J. Appl. Phys.* **1999**, *86*, 2660.

[40] B. Liu, W. Zhao, Z. Ding, I. Verzhbitskiy, L. Li, J. Lu, J. Chen, G. Eda, K. P. Loh, *Adv. Mater.* **2016**, *28*, 6457.

[41] P. Wangyang, H. Sun, X. Zhu, D. Yang, X. Gao, *Mater. Lett.* **2016**, *168*, 68.

[42] W. Zheng, Z. Zhang, R. Lin, K. Xu, J. He, F. Huang, *Adv. Electron. Mater.* **2016**, *2*, 1600291.

[43] H. Li, Z. Yin, Q. He, H. Li, X. Huang, G. Lu, D. W. Fam, A. I. Tok, Q. Zhang, H. Zhang, *Small* **2012**, *8*, 63.

[44] X. Lu, M. I. B. Utama, J. Lin, X. Luo, Y. Zhao, J. Zhang, S. T. Pantelides, W. Zhou, S. Y. Quek, Q. Xiong, *Adv. Mater.* **2015**, *27*, 4502.

[45] M. Yagmurcukardes, F. M. Peeters, H. Sahin, *Phys. Rev. B* **2018**, *98*, 085431.

[46] C. Cong, J. Shang, L. Niu, L. Wu, Y. Chen, C. Zou, S. Feng, Z.-J. Qiu, L. Hu, P. Tian, Z. Liu, T. Yu, R. Liu, *Adv. Opt. Mater.* **2017**, *5*, 1700609.

[47] I. Baltog, M. Baibarac, S. Lefrant, *J. Phys.: Condens. Matter* **2009**, *21*, 025507.

[48] M. H. Chiu, M. Y. Li, W. Zhang, W. T. Hsu, W. H. Chang, M. Terrones, H. Terrones, L. J. Li, *ACS Nano* **2014**, *8*, 9649.

[49] X. Zhang, X. F. Qiao, W. Shi, J. B. Wu, D. S. Jiang, P. H. Tan, *Chem. Soc. Rev.* **2015**, *44*, 2757.

[50] H. Li, J. B. Wu, F. Ran, M. L. Lin, X. L. Liu, Y. Zhao, X. Lu, Q. Xiong, J. Zhang, W. Huang, H. Zhang, P. H. Tan, *ACS Nano* **2017**, *11*, 11714.

[51] K. G. Zhou, F. Withers, Y. Cao, S. Hu, G. Yu, C. Casiraghi, *ACS Nano* **2014**, *8*, 9914.

[52] M. Buscema, G. A. Steele, H. S. J. van der Zant, A. Castellanos-Gomez, *Nano Res.* **2014**, *7*, 561.

[53] S. Sahoo, A. P. S. Gaur, M. Ahmadi, M. J. F. Guinel, R. S. Katiyar, *J. Phys. Chem. C* **2013**, *117*, 9042.

[54] L. Liang, J. Zhang, B. G. Sumpter, Q. H. Tan, P. H. Tan, V. Meunier, *ACS Nano* **2017**, *11*, 11777.

[55] M. D. Tran, J. H. Kim, H. Kim, M. H. Doan, D. L. Duong, Y. H. Lee, *ACS Appl. Mater. Interfaces* **2018**, *10*, 10580.

[56] G. Kresse, J. Furthmüller, *Phys. Rev. B* **1996**, *54*, 11169.

[57] J. P. Perdew, K. Burke, M. Ernzerhof, *Phys. Rev. Lett.* **1996**, *77*, 3865.

[58] A. D. Becke, *Phys. Rev. A* **1988**, *38*, 3098.

[59] Y. Gong, J. Lin, X. Wang, G. Shi, S. Lei, Z. Lin, X. Zou, G. Ye, R. Vajtai, B. I. Yakobson, H. Terrones, M. Terrones, B. K. Tay, J. Lou, S. T. Pantelides, Z. Liu, W. Zhou, P. M. Ajayan, *Nat. Mater.* **2014**, *13*, 1135.